TIME-DELAY SYSTEMS WITH BAND-LIMITED FEEDBACK

Lucas Illing
Dept of Physics and CNCS
Duke University
United States of America
illing@phy.duke.edu

J. N. Blakely
U. S. Army Research, Development,
and Engineering Command
Redstone Arsenal
United States of America
Jonathan.Blakely@us.army.mil

Daniel J. Gauthier
Dept of Physics and CNCS
Duke University
United States of America
gauthier@phy.duke.edu

Abstract

Fast nonlinear devices with time-delayed feedback, developed for applications such as communications and ranging, typically include components that are AC-coupled, i.e. components that block zero frequencies. As an example of such a system, we describe a new opto-electronic device with band-limited feedback that uses a Mach-Zehnder interferometer as passive nonlinearity and a semiconductor laser as a current-to-optical-frequency converter. Our implementation of the device produces oscillations in the frequency range of tens to hundreds of MHz. We observe periodic oscillations created through a Hopf bifurcation as well as quasiperiodic and high dimensional chaotic oscillations. Motivated by the experimental results, we investigate the steady-state solution and it's bifurcations in time-delay systems with band-limited feedback and arbitrary nonlinearity. We show that the steady state loses stability, generically, through a Hopf bifurcation, which can be either supercritical or subcritical. As a result of this investigation, we find that band-limited feedback introduces practical advantages, such as the ability to control the characteristic time-scale of the dynamics, and that it introduces differences to Ikeda-type systems already at the level of steady-state bifurcations, e.g. bifurcations exist in which limit cycles are created with periods other than the fundamental "period-2" mode found in Ikeda-type systems.

Key words

Bifurcation, chaos, delayed-feedback system, opto-electronic devices, time-delay systems.

1 Introduction

Time-delay devices operating in the radio-frequency (RF) regime are widely used as generators of chaos in applications such as communication, chaos control, and ranging. As an example, such devices are studied as a signal source for future radar applications because chaotic waveforms have the desirable properties of a large frequency-bandwidth and a fast decay of correlations [Lukin, 1997; Myneni, 2001]. Furthermore, time delayed feedback is used in the chaos control scheme known as time-delay autosynchronization [Pyragas, 1992; Socolar, 1994]. Additionally, microwave [Mykolaitis, 2003; V. Dronov], opto-electronic [Abarbanel, 2001; Goedgebuer, 2002; Goedgebuer, 2004; Blakely, 2004a], and optic [VanWiggeren, 1998; Fischer, 2000; Kusumoto, 2002] time-delay devices are considered for communication systems since they can generate chaos with frequencies that match the frequency range of the communication infrastructure and provide advantages such as increased privacy [Goedgebuer, 2004] and high power efficiency [V. Dronov].

At high speed, many components are AC-coupled, which means that low frequency signals are suppressed in devices that include such components. As a consequence, the time-delayed feedback signal is band-pass filtered because, in addition to the cut off at low frequencies, high frequencies are suppressed due to the finite response time of device components.

Time-delay dynamical system with band-limited feedback have recently received increased attention because they have the advantage that the bandwidth of the chaotic signal can be tailored to fit a desired communication band [Goedgebuer, 2002; Goedgebuer, 2004] and they have flexible dynamical time scales because adjusting the band-pass characteristics of the feedback loop allows tuning of the characteristic frequencies [Blakely, 2004a].

In this paper we investigate time-delay systems with band-limited feedback both experimentally and theoretically.

We describe a new fast optical device that belongs to the class of optical systems with passive nonlinearity and band-limited feedback in Sec. 2 of this paper. In our device a Mach-Zehnder interferometer is the source of nonlinearity while the semiconductor laser that provides the optical power acts as a linear current-to-optical-frequency converter. The nonlinearity of the interferometer coupled with the delay in the feedback

loop combine to produce a range of steady state, periodic, and chaotic behavior.

Motivated by the experimental findings, we take a first step in a rigorous study of time-delay systems with band-limited feedback by investigating the steady-state bifurcations for arbitrary nonlinearities. In Sec. 3 we derive expressions for the instability boundary and show that the steady state becomes unstable, generically, through a Hopf bifurcation. Distinguishing dynamical features that arise because of the AC-coupled components are also discussed.

2 Experimental Results

In this section we present details about the experimental implementation of our opto-electronic device and provide a simple a model that permits quantitative predictions about the device dynamics. We investigate the nonlinear dynamics of the system through a combination of experimental observations and numerical computation. A good understanding of the system dynamics is a prerequisite for the development of applications such as control of fast chaos, which will be reported elsewhere [Blakely, 2004b].

To characterize the device, we measure the critical gain at which the device-dynamics transitions from steady state to oscillatory behavior and determine the oscillation frequency. Furthermore, we present evidence that our opto-electronic device generates chaos for large feedback gain.

2.1 Experimental setup

First, we describe details of the experimental implementation of the active laser interferometer with AC-coupled feedback. The device consists of the laser, that acts a current controlled source, the interferometer, that constitutes the passive nonlinearity in the system, and the feedback loop with bandpass characteristics. A schematic of the experimental setup is shown in Fig. 1.

The light source is an AlGaInP diode laser (Hitachi HL6501MG, wavelength 0.65 μm) with a multi-quantum well structure. The diode is equipped with a bias-T for adding an RF component to the injection current. Thermoelectric coolers are used to provide 1 mK temperature stability thereby minimizing frequency and power drift. The output light of the laser is collimated by a lens (Thorlabs C230TM-B, f=4.5mm) producing an elliptical beam (1 mm × 5 mm) with a maximum output power of 35 mW. The relaxation oscillation frequency of the laser at the nominal operating current of 75 mA is $\Omega_R = 2.7$ GHz.

The passive nonlinearity in the experiment consists of a Mach-Zehnder interferometer with unequal path lengths (path difference 45 cm) into which the laser beam is directed. A silicon photodetector (Hammamatsu S4751, DC-750 MHz bandwidth, 15 V reverse bias) measures the intensity of light emitted from one output port of the interferometer. The size of the photodiode is much smaller than the width of the laser
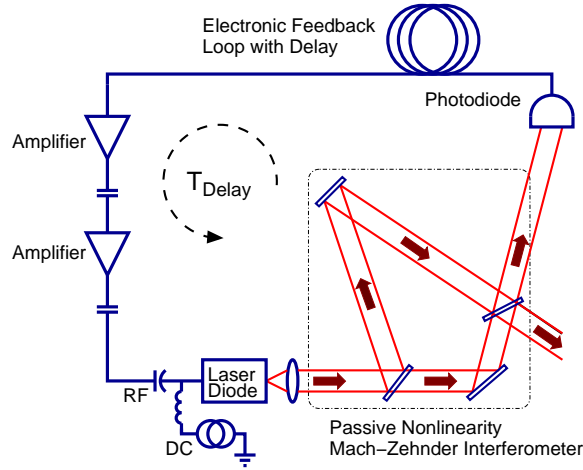

Figure 1. Schematic of experimental setup. The device consists of a voltage controlled source, a passive nonlinearity, and a feedback loop with bandpass characteristics. Details of the setup are explained in the text.

beam so only a fraction of the interferometer's output is detected. The small detector size ensures that only one fringe appears within the beam cross section thus compensating for wavefront aberrations and slight laser beam misalignment and improving the fringe visibility.

The feedback-loop photodiode produces a current proportional to the optical power falling on its surface. The current is converted to a voltage (using a 50Ω resistor) and is transmitted down a coaxial cable (RU 58, total length ~ 327 cm). The signal emanating from the cable passes through an AC-coupled amplifier (MiniCircuits ZFL-1000LN, bandwidth 0.1-1000 MHz), a DC-blocking chip capacitor (220 pF), a second AC-coupled amplifier (Mini-Circuits ZFL-1000GH, bandwidth 10-1200 MHz), and a second DC-blocking chip capacitor (470 pF). The capacitors reduce the loop gain at frequencies below ~ 7 MHz where a thermal effect enhances the laser's sensitivity to frequency modulation [Kobayashi, 1982; Tsai, 1999]. The resulting voltage is applied to the bias-T in the laser mount. The bias-T converts the signal into a current and adds it to a DC injection current from a commercial laser driver (Thorlabs LDC500).

2.2 Model of the opto-electronic device

The following delay-differential equation (DDE) can be derived by considering the relevant physics of the laser diode, the Mach-Zehnder interferometer, and the feedback loop components [Blakely, 2004a]:

$$\begin{aligned} \tau_h \dot{P}(\tilde{t}) &= -\left(P(\tilde{t}) - P_0\right) + \tau_h \kappa \dot{V}(\tilde{t}), \\ \tau_l \dot{V}(\tilde{t}) &= -V(\tilde{t}) + \gamma\, G\left[P(\tilde{t} - T_D)\right], \end{aligned} \tag{1}$$

with

$$G\left[P\right] = P\left\{1 + \beta\, \sin\left[\alpha\,\left(P - P_0\right)\right]\right\}. \tag{2}$$

In this model $V(\tilde{t})$ is the voltage in the electronic feedback loop, $P(\tilde{t})$ denotes the laser's emission power, and P_0 is the laser power at steady state. All parameters of the model can be measured and are given in Table I in Ref. [Blakely, 2004a].

Equation (1) models the band-limited transfer characteristics of the electronic feedback loop as a two-pole bandpass filter, where the time-scale τ_h is related to the corner frequency of the high-pass filter through $\omega_h = \tau_h^{-1}$ and τ_l is related to the corner frequency of the low-pass filter through $\omega_l = \tau_l^{-1}$. The gain due to the amplifiers is given by γ. The total time-delay is T_D.

In the experiment, the laser acts as a linear device that converts input-voltage oscillations to frequency oscillations due to the following mechanism. The injection current applied to the laser diode is a combination of the DC-bias current and the high-frequency currents due to the time-delayed output of the feedback loop. Modulating semiconductor lasers by varying the input current results primarily in changes of the laser frequency and, to a lesser extent, the laser power. One physical process relating the input current and frequency shifts is the change of carrier density in the laser device as result of the modulation. A changed carrier density shifts the refractive index of the material that makes up the laser cavity and thereby changes the frequency of the lasing mode. Due to the bandpass-limited feedback in our experiment, the pumping current is modulated at a rate significantly slower than the nanosecond internal timescale of the laser ($\Omega_R = 2.7$ GHz) and hence the optical frequency will adiabatically follow the pumping current. Thus, the laser is a linear voltage-to-frequency converter, which is characterized by the conversion strength κ.

The nonlinearity in the experiment is due to the unequal pathlength Mach-Zehnder interferometer and is given by Eq. (2). In Eq. (2), the parameter β is the fringe visibility and α determines the interferometer sensitivity.

Model (1) is used for quantitative comparison between numerical predictions and measured quantities such as the laser power. However, for theoretical studies, it is convenient to bring Eq. (1) in a simpler form by introducing the rescaled and dimensionless variables $t = \tilde{t}(\tau_h^{-1} + \tau_l^{-1})$, $x = (P - P_0)/P_0$, and $y = \tau_h(\tau_h + \tau_l)^{-1}\{(P - P_0) - \kappa(V - \gamma G[0])\} P_0^{-1}$. Using these dimensionless variables we obtain the following model:

$$
\begin{aligned}
\frac{dx(t)}{dt} &= -x(t) + y(t) + b\,\frac{f[x(t - \tau)]}{f'(0)}, \\
\frac{dy(t)}{dt} &= -r\,x(t).
\end{aligned} \tag{3}
$$

Here, the dimensionless delay is $\tau = T_D\,(\tau_l^{-1} + \tau_h^{-1})$, $r = \tau_l\tau_h(\tau_l + \tau_h)^{-2}$, and the nonlinear delay term f of (3) is defined as $f(x(t - \tau)) = \tau_h(\tau_l + \tau_h)^{-1}\{G[P_0(x(t - \tau) + 1)] - G[P_0]\} P_0^{-1}$
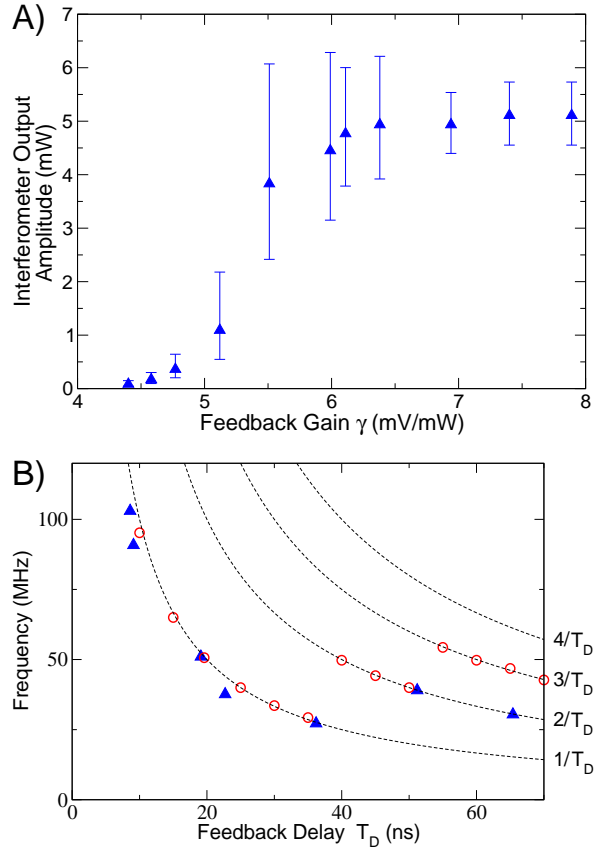

Figure 2. Hopf bifurcation of the steady state. A) Scaling of the oscillation amplitude as the feedback gain is varied. B) Scaling of the limit-cycle frequency close to instability threshold as a function of of the delay.

and is given by

$$
f(x) = \frac{\tau_h}{\tau_h + \tau_l}\,(x + \beta\,x\,\sin(a\,x) + \beta\,\sin(a\,x)). \tag{4}
$$

The parameter b denotes the effective slope of the nonlinearity, *i.e.* the total feedback-gain for small signals, and is defined as $b = \kappa\gamma f'(0)$. The fixed parameters of model (3) that correspond to the measured device-parameters [Blakely, 2004a] are given by $\tau = 29.8$, $r = 0.028$, $a = \alpha P_0 = 49.14$, $\tau_h = 22$ ns, $\tau_l = 0.66$ ns, and $\beta = 0.8$.

There are three dimensionless parameters that influence the dynamics: the effective slope b (proportional to the gain γ), the strictly positive delay τ, and r ($0 < r \le 1/4$). The parameter r is related to the angular frequency at which the transfer-function of the bandpass-filter is maximum. Indeed, the frequency that maximizes transmission is $\omega_{max} = \sqrt{\omega_l\omega_h}$, which, in the new variables, corresponds to the dimensionless angular frequency $\Omega_{max} = \sqrt{r}$.

2.3 Hopf-Bifurcation

Our device can display very complex dynamics. As system parameters are varied we observe steady state behavior, periodic and quasiperiodic oscillations as

well as chaotic dynamics. In this section we discuss the transition from steady state to periodic behavior.

We know of no exhaustive list that contains all bifurcations through which limit cycles (periodic oscillations) can arise in time-delay systems. However, for those limit-cycle bifurcations that already exist in two-dimensional systems, this list exists. Furthermore, the different bifurcation scenarios in this list can be distinguished by examining the scaling of the period and amplitude near the bifurcation point [Strogatz, 1994]. For instance, a supercritical Andronov-Hopf bifurcation is characterized by an amplitude of the stable limit cycle that scales as the square-root of the distance of the bifurcation parameter from the bifurcation point and an oscillation period of finite size that is approximately constant as the bifurcation parameter is varied.

To investigate the bifurcations in the system, we varied the feedback gain γ and the delay time T_D. Experimentally, we can change T_D by adding or subtracting fixed lengths of coaxial cable to the feedback loop.

First we vary the gain for fixed $T_D \sim 19.1$ ns. For gain values below a critical value $\gamma < \gamma_C$ the system is in a steady state with fluctuations of the observed laser output power due only to the inherent phase noise. When the gain is increased through the critical value $\gamma_C = 5.1 \pm 0.5$ mV/mW the steady state is replaced by a periodic oscillation. The dominant frequency of the oscillation is 51.5 ± 1 MHz, which is roughly equal to $1/T_D$. This frequency does not change much as the gain is further increased. On the other hand, the amplitude grows smoothly from zero with increasing gain. Figure 2A shows the amplitude growth measured in the experiment. The spontaneous emission noise of the semiconductor laser leads to an amplification of the amplitude variations (larger error bars) close to the bifurcation [Garcia-Ojalvo, 1996]. It is therefore not possible to pinpoint the bifurcation point exactly and there is no clear $\sqrt{\gamma - \gamma_C}$ scaling of the amplitude. Nevertheless, the smooth amplitude growth and the finite period of the limit cycle at $\gamma \gtrsim \gamma_C$ indicate a supercritical Andronov-Hopf bifurcation at γ_C. In the noise-free model, we find an Andronov-Hopf bifurcation at $\gamma_C = 5.34$ mV/mW.

Next, we experimentally determined the frequency of the limit cycle close to the bifurcation point for different delay times T_D. In all cases the steady state becomes unstable through an Andronov-Hopf bifurcation. However, we find that the relation $f \sim 1/T_D$ between the frequency f and the delay time T_D holds only for a limited range of T_D. Figure 2B summarizes the relation between f and T_D that we obtain from experimental (triangles) and numerically calculated (circles) time series. The data suggest that the device transitions from a steady state to limit cycle oscillations with frequencies roughly n/T_D, where $n = n(T_D)$ can be $1, 2, 3, \ldots$.

All of the above experiments were conducted for positive feedback-gain. In the experiment, it is also possible to achieve negative gain [Blakely, 2004a]. For negative
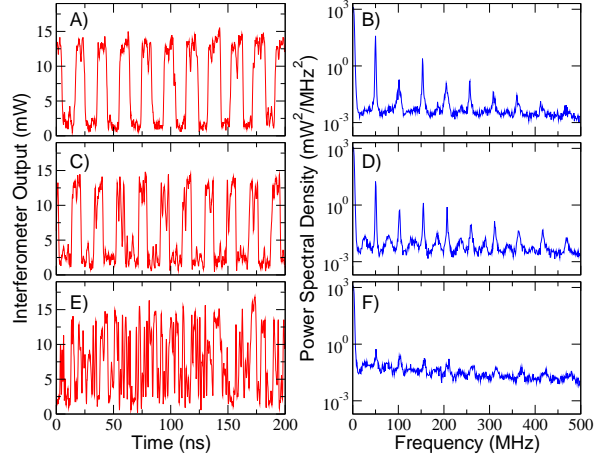

Figure 3. Experimentally measured timeseries (panels A,C,E) and power spectra (panels B,D,F) obtained from the second output port of the interferometer are shown. For $\gamma = 9.4$ mV/mW for A) and B), $\gamma = 13.2$ mV/mW for C) and D), and $\gamma = 17.6$ mV/mW for E) and F).

gain, we observe that $f \sim 1/(2\,T_D)$ for delay times of $T_D = 19.1$ ns.

2.4 Chaos

Beyond the Hopf bifurcation, successively more complex dynamics develops as the gain is increased. Figure 3 shows a series of time traces and power spectra. We measured the power spectral density when the gain is just below the Hopf bifurcation to obtain an estimate of 2×10^{-3} mW^2/MHz^2 for the noise floor. Spectral features weaker than this level are completely obscured in the experiment. At feedback gains higher than the Andronov-Hopf bifurcation point, the initially sinusoidal oscillations begin to square off, as shown in Fig. 3A. The square shape of the waveform results in prominent odd harmonics in the spectrum Fig. 3B. As the gain is increased, a small, broad peak appears at about half the fundamental frequency as shown in Fig. 3D. The peak at roughly half the fundamental frequency is three orders of magnitude below the fundamental. The weakness and broadness of this peak coupled with the presence of phase noise may explain why no period doubled behavior is apparent in the time domain Fig. 3C. As the gain is further increased, the broad background rises and the tall peaks at the fundamental frequency and its harmonics weaken. The power spectrum for $\gamma = 17.6$ mV/mW, shown in Fig. 3F, is quite broad and the peaks have nearly dropped to the level of background. This is indicative of high dimensional chaos in the system.

A similar very broad and featureless power spectrum in the chaotic regime for an optical system with passive nonlinearity and bandpass feedback was reported in [Goedgebuer, 2002], where the authors also synchronize two of their devices and successfully communicate information. The ability to synchronize can be interpreted as a demonstration that the cause of the broad-

band spectrum is deterministic chaos. Because of the similarity of their system to ours, we believe the same to be true for our system. The observed complex behavior for large gain values is due to chaotic deterministic dynamics.

To support this claim we show time series and power spectra obtained by numerical simulation of the noise-free model. The match with the experimental data is good, as can be seen by comparing Fig. 3 to Fig. 4. The Poincaré sections of Fig. 4 are obtained by recording the location where the trajectory uni-directionally crosses a fixed plane ($V(t) = V_0$) in the three dimensional space spanned by $(V(t), P(t), P(t - \Delta t)$ with $\Delta t < T_D$. The numerics confirm that the system is on a limit cycle for $\gamma = 9.4$ mV/mW, which is clear from the power spectrum (Fig. 4B) and immediately obvious in the Poincaré section (Fig. 4C). The noise-free simulations show that the limit cycle has bifurcated to a torus-attractor for increased gain ($\gamma = 13.2$ mV/mW), appearing as closed curve in the Poincaré section (Fig. 4F). The power spectrum, Fig. 4E, exhibits a comb-like structure due to the two incommensurate frequencies of the quasi-periodic oscillation. It should be noted, that there is not only a strong peak at ~26.6 MHz (roughly half the fundamental frequency) but also a definite peak at 1.8 MHz, which is well below the 3 dB cutoff point of the high-pass filter. At present, we do not understand the origin of this low frequency.

Increasing the gain even further, leads through a series of complicated bifurcations, that we did not analyze in detail, to the creation of a chaotic attractor, characterized by a very broadband spectrum (Fig. 4H) and no discernible structure in the Poincaré section. The largest Lyapunov exponents at a gain of $\gamma = 17.6$ mV/mW are clearly positive. Based on the numerical computation of the largest Lyapunov exponents at this gain-value, we obtain an estimate of the attractor's Lyapunov dimension of $D_L \sim 22$.

In summary, using experimental measurements and numerical computation of the model we show that high dimensional chaos exists in our device. As the feedback gain is increased, the chaotic attractor is created through a rather complex series of bifurcations, the initial stages of which are: steady state → limit cycle → torus → ... → chaos.

3 Theory

In Sec. 2, we described an opto-electronic device that can produce high-dimensional chaos. The characteristic time scales of the oscillations can be adjusted by changing the bandpass characteristics in the feedback loop. We also showed that the device-dynamics is well described by a DDE (Eq. (1) or Eq.(3)). This DDE is related to Ikeda-type DDEs [Ikeda, 1987] but extends the Ikeda model by including high-pass filter transfer characteristics of the feedback in addition to the low-pass filter characteristics considered by Ikeda.

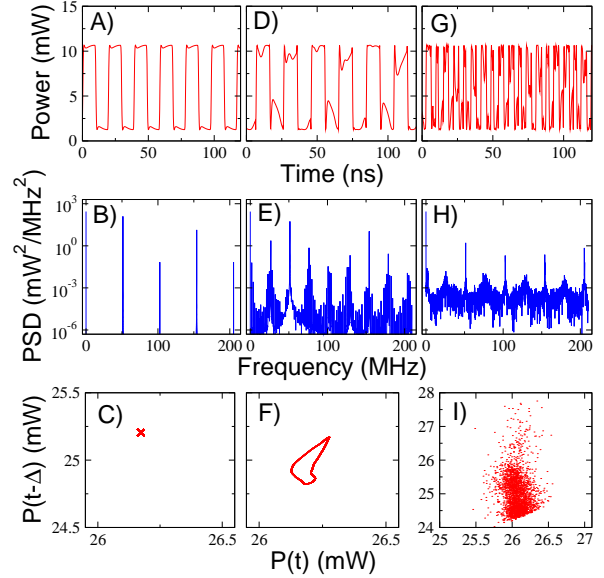In designing devices, it is useful to have theoretical

Figure 4. Numerical timeseries (panels A,D,G), power spectra (panels B,E,H), and Poincaré sections (panels C,F,I) are shown. The gain values are as in Fig.3, that is, $\gamma = 9.4$ mV/mW (A,B,C), $\gamma = 13.2$ mV/mW (D,E,F), and $\gamma = 17.6$ mV/mW (G,H,I).

insights concerning the possible dynamics and the bifurcation scenarios that one might expect. Questions that are of practical interest include: For which parameter values is the steady state stable and what are the bifurcations of the steady state? What determines the frequency and stability of periodic oscillations? Is the system multi-stable? Is the chaotic attractor in these system robust with respect to parameter variations?

For time-delay devices with passive nonlinearity and DC-coupled feedback, *i.e.* devices that can be model through scalar DDEs of Ikeda-type, many of these questions have been addressed both experimentally [Derstine, 1983; Liu, 1991; Goedgebuer, 1998] and theoretically [Ikeda, 1979; Nardone, 1986; Ikeda, 1987; Hale, 1996; Giannakopoulos, 1999; Nizette, 2004; Erneux, 2004], starting in 1979 with the pioneering work of Ikeda [Ikeda, 1979]. On the other hand, for DDEs of the form of Eq. (3), a similarly rigorous study remains to be done.

In this section we take a first step in the direction of a rigorous mathematical analysis of time-delay systems with band-limited feedback by analyzing the bifurcations from the steady-state solution of model (3) for arbitrary nonlinearities f.

3.1 Characteristic Equation

We use linear stability analysis to investigate the local stability of the trivial solution $x = y = 0$. The trivial solution is the only steady state solution of Eq. (3). The main idea is to ask how small perturbations to the trivial solution evolve for a given set of parameter values, which is equivalent to studying the corresponding characteristic equation [Hale, 1993; Hale, 2002]. The

characteristic equation of model (3) is

$$\lambda^2 + \lambda + r - b\lambda e^{-\lambda\tau} = 0, \qquad (5)$$

where the effective slope b (proportional to the feedback gain) is one of the relevant bifurcation parameters of the problem. The delay τ is the second relevant bifurcation parameter.

To determine the local stability of the fixed point, we consider solutions of (5), which is transcendental and has an infinite number of roots λ for every set of parameters. The steady state is locally stable if all roots (eigenvalues) have a negative real part. Thus, to determine parameter values for which the fixed point becomes unstable, we set $\mathrm{Re}(\lambda) = 0$ and $\mathrm{Im}(\lambda) = i\Omega$. Separating real and imaginary part yields

$$\begin{aligned} 0 &= -\Omega^2 + r - b\Omega\sin(\Omega\tau), \\ 0 &= 1 - b\cos(\Omega\tau). \end{aligned} \qquad (6)$$

We find that all roots of Eq. (6) have nonzero frequency Ω and occur in complex conjugate pairs ($\lambda = \pm i\Omega$). Thus, generically, a Hopf bifurcation occurs.

One way to visualize the solution of (6) is to seek parameterized curves in the plane of two bifurcation parameters, which we choose as the delay τ and the effective slope b. Since only Hopf bifurcations occur in our system, we will refer to these curves as Hopf curves. The Hopf curves separate regions in parameter space with different numbers of eigenvalues in the right complex halfplane. The relevant region where the fixed point is stable (no eigenvalues in the right complex halfplane) is the one that includes $\gamma = b = 0$. The parameterization of the Hopf curves is most conveniently achieved by introducing a new variable $s = \Omega\tau$, yielding

$$\begin{aligned} \tau_C^n(s) &= \frac{s}{2r}\left(\tan(s) + \sqrt{\tan^2(s) + 4r}\right) \\ b_C^n(s) &= \frac{1}{\cos(s)}. \end{aligned} \qquad (7)$$

Here, the label n denotes the different solution branches. For $n \in \mathbb{N}^+$ the parameterization variable s is in the range $(2n-1)\pi/2 < s < (2n+1)\pi/2$, and $0 < s < \pi/2$ for the branch with $n = 0$. Note that b_C^n is positive for even n and negative for odd n.

In Fig. 5A, the stability boundary of the fixed point is shown in parameter space. It is seen, that the trivial solution is always locally stable if $-1 < b < 1$, independent of the delay τ. Furthermore, for large delays, $|b_C| \approx 1$ becomes an increasingly accurate approximation of the stability boundary. On the other hand the trivial solution may be stable for a considerably larger range of the bifurcation parameter, for small delays τ.
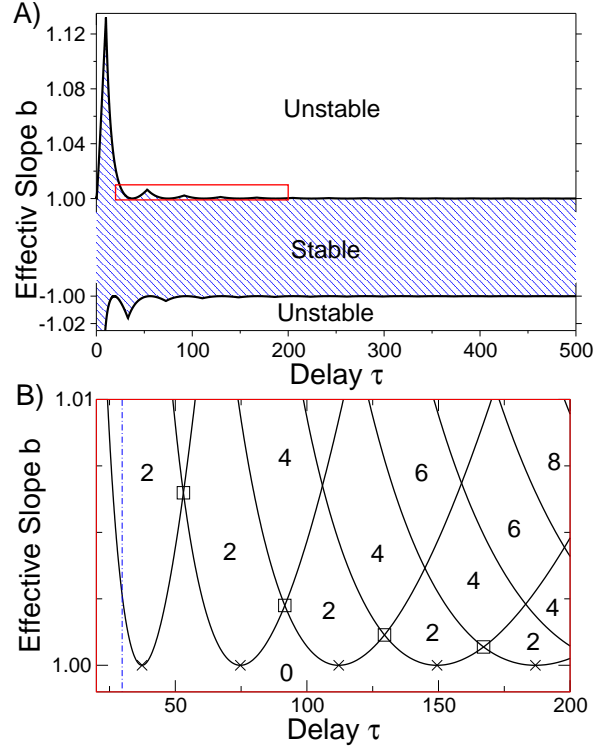

Figure 5. A) In the space formed by the delay and the effective slope we display in blue the region of local stability. Note that a large part of the stability region ($-1 < b < 1$) has been contracted in order to make details of the boundary visible. B) A detailed look is provided at a portion of the stability boundary (red box in panel A) which is formed by combining appropriate parts of the Hopf-curves $\left(\tau_C^n(s), b_C^n(s)\right)$. The full extent of these curves is shown as solid lines (starting from the left the curve-index n is $n = 2, 4, 6, 8, \ldots$). The Hopf-curves delimit regions in parameter space for which there is a constant number eigenvalues in the right complex halfplane. This number is also given. The square symbol marks points on the stability boundary where two pairs of complex conjugate eigenvalues lie on the imaginary axis, whereas crosses denote the extrema of the Hopf-curves, i.e. $b = 1$. The blue dashdotted line indicates the delay that was used in the experiment (see Fig. 2A, Fig. 3, and Fig. 4).

Figure 5B provides a zoomed-in view of part of the parameter-space where the boundary and the full extent of the parameterized curves $\left(\tau_C^n(s), b_C^n(s)\right)$ are depicted. It can be shown that the pairs of simple characteristic roots of Eq. (5) always cross the imaginary axis transversally [Illing]. Therefore, the number of eigenvalues in the right complex halfplane can easily be determined by counting how many of Hopf curves are crossed. This number is indicated in Fig. 5B. Furthermore, there is exactly one pair of roots on the imaginary axis for all parameter combinations of b and τ that fall on one of the Hopf-curves. The exception are points where two Hopf-curves intersect, because two pairs of eigenvalues cross into the right halfplane in that case and a codimension-two bifurcation (double-Hopf bifurcation) occurs. The location of double-Hopf points is indicated in Figure 5B by square symbols.
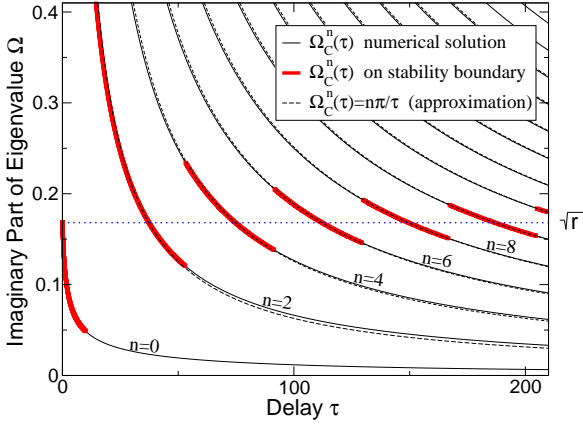
Figure 6. Imaginary part of the eigenvalue versus the delay. $\Omega_C^n(\tau)$ is shown for positive b (n is even) and $r = 0.028$. The part of each branch n that belongs to the stability boundary is shown as bold red line. The dashed lines are an approximation (see text).

In Figure 5B the blue dash-dotted line indicates the delay at which the critical gain was determined in the experiment (see Fig. 2A). From the theory we obtain $b_C = 1.003$, which corresponds to a feedback-gain $\gamma = 5.34$ mV/mW, in agreement with the experimental result of $\gamma_C = 5.1 \pm 0.5$ mV/mW.

The main result of above linear stability analysis is the steady state will lose it's stability, generically, through a Hopf bifurcation in time-delay systems with band-limited feedback. This result is independent of the specific form of the nonlinearity f. Additionally, we find that double-Hopf points exist along the stability boundary. In experiments, the chance of choosing the delay so that the stability boundary will be crossed close to a double-Hopf point is negligible. However, it is known that double-Hopf interactions lead to limit cycles as well as tori and chaos [Guckenheimer, 1983]. The existence of double-Hopf points therefore indicates that quasi-periodic and chaotic dynamics might occur in such systems, in agreement with our experimental findings.

3.2 Frequency

So far we have discussed the conditions under which the steady state is stable. That is, we have shown how to calculate the critical gain γ_C for known values of the delay (τ), the first derivative of the nonlinearity ($f'(0)$), and the frequency of maximal transmission ($\sqrt{r}$). The value of γ_C can be compared with experiments. Another useful way to compare experiments and theory is to study the frequency of oscillations at the onset of instability.

Consider the case where the Hopf bifurcation is supercritical. In this case, as the stability boundary is crossed, the fixed point becomes unstable, a stable limit cycle is born, and the system starts to oscillate. Experimentally the frequency of oscillation is the quantity that is most readily measured. The frequency at onset, denoted by f_C^n, is determined by Ω_C^n through

$f_C^n = \Omega_C^n (2\pi)^{-1}(\omega_h + \omega_l)$. Therefore, it is useful to plot the eigenvalue Ω_C^n versus the delay τ as is done in Fig. 6.

The frequency scales roughly as $\Omega_C^n \sim n\pi/\tau$ ($f_C^n \sim n/(2\tau)$) for $n > 0$ in the vicinity of the extrema of the Hopf curves (crosses in Fig. 5B), $|b_C^n| = 1$, $\Omega_C^n = \sqrt{r}$). This scaling of the frequency is shown in Fig. 6 using dashed lines and is explained by considering whether a wave circulating in the feedback loop will reinforce itself. For the case of positive feedback ($b > 0$) a periodic perturbation will reinforce itself, if the feedback delay is a multiple of the wave's period, i.e. $f \sim n/(2\tau)$ with n an even integer. On the other hand, a sinusoidal perturbation is amplified by negative feedback ($b < 0$), if it is shifted by half it's period after one round-trip. Thus, for $b_C < 0$ the frequency is expected to scale as $f \sim n/(2\tau)$ with n an odd integer. This reasoning is consistent with the fact that for n even (odd) the critical effective slope b_C^n is positive (negative).

From Fig. 6, it is seen also that different oscillation "modes" will be observed as τ is increased. That is, the frequency of the observed oscillations will jump from $f \sim n/(2\tau)$ to $f \sim (n+2)/(2\tau)$ as τ is varied across one of the double-Hopf points; squares in Fig. 5B. These jumps are explained by the fact that the gain in the feedback loop is not perfectly flat over the pass-band. As b is increased from a low level, one particular frequency will first reach the threshold where the gain in the loop balances the losses. In a system with only low-pass feedback, the gain is highest at low frequencies, so the oscillation-mode with the lowest frequency is always the one that destabilizes the steady state, independent of the delay. On the other hand, the high-pass filter introduces a bias toward high frequencies. Because the frequency scales roughly as $f_C^n \sim \tau^{-1}$ for each mode n, the damping effect of the high pass filter on a particular mode becomes more pronounced with increasing delay time τ. Therefore, there exists a delay τ for which a higher order mode, one that has a higher frequency for a given delay, will reach threshold first.

Thus, the scaling of the frequency of the limit-cycles that we observed in the experiment (see Fig. 2) is not specific to our device but rather a general feature of any time-delay systems with band-limited feedback. In this context, recall that the limit cycle at onset for Ikeda-type DDEs is always the fundamental "period-2" mode, with a frequency $f \sim (2\tau)^{-1}$ for large delays ($\tau \gg \tau_l$) [Nardone, 1986; Erneux, 2004]. Since high-pass filtering, in contrast, results in a stability boundary where the mode at threshold varies with the chosen delay, it is possible to experimentally distinguish time-delay systems with band-limited feedback from systems with low-pass feedback by examining the frequency of the oscillations at the onset of instability as a function of the delay.

3.3 Hopf bifurcation type

In the previous sections, we have shown that a time-delay system with band-limited feedback undergoes Hopf bifurcations as the system parameters are varied. However, we have not yet determined whether the Hopf bifurcations are subcritical or supercritical. The expected dynamical behavior close to threshold is very distinct for the two bifurcation types. For a supercritical Hopf bifurcation, one expects small amplitude sinusoidal oscillations past the critical gain, whereas for a subcritical bifurcation, one expects bistability and hysteresis close to the bifurcation point.

One way to determine the type of bifurcation is through the use of center manifold techniques and normal form theory. Normal forms have been studied extensively for finite-dimensional ordinary differential equations (ODEs) [Guckenheimer, 1983]. Recently, normal-form theory was developed for the case of DDEs [Faria, 1995], which may be applied to model (3) to show that both subcritical and supercritical Hopf bifurcations can occur, depending on the parameters [Illing].

For a fixed delay τ and r, the critical effective slope b_C^n and Ω_C^n are uniquely determined for each of the Hopf curves with label n. For given $\tau, r, b_C^n(r, \tau)$, and $\Omega_C^n(r, \tau)$, it is possible to derive a criterion that determines the Hopf-bifurcation type based on the knowledge of the second and third derivative of the nonlinear function, *i.e.* $f''(0)$ and $f'''(0)$. To state this criterion we define

$$N^n = [r + \Omega^2][b^4 + 2b^3 + b^2 - 4] +$$
$$+ \, \text{sgn}(\tau - \frac{n\pi}{\sqrt{r}}) 3\Omega\sqrt{b^2 - 1}[(4 - b^2)(r + \Omega^2) + 2\Omega^2\tau b^2]$$
$$+ 2\Omega^2\tau b^2[b^3 - 1]$$

and

$$C^n(\tau, r) = \frac{-2\Omega^2 b^{-1}}{(b^2\Omega^2\tau + r + \Omega^2)} \, N^n \cdot$$
$$\cdot \left| 2i\Omega b + (4\Omega^2 - 2i\Omega - r)e^{2i\Omega\tau} \right|^{-2}. \tag{8}$$

Here, $b = b_C^n$ and $\Omega = \Omega_C^n$ is used for notational convenience. It can be then be shown [Illing] that

Proposition 1. *For $r, \tau \in \mathbb{R}^+$, $r \leq \frac{1}{4}$, and $n = 0, 1, 2, \dots$:*
• *If $f'(0) f'''(0) + f''(0)^2 C^n(\tau, r) > 0$, the Hopf bifurcation is subcritical.*
• *If $f'(0) f'''(0) + f''(0)^2 C^n(\tau, r) < 0$, the Hopf bifurcation is supercritical.*

Since the Taylor-series coefficients of f are known, the difficulty in determining whether the Hopf-bifurcation is subcritical or supercritical is shifted to finding the value of $C^n(\tau, r)$. Two simple cases that arise in this context are the following:

Corollary 2.

(1) *There are no quadratic terms in the Taylor expansion of the nonlinearity ($f''(0) = 0$): Therefore, if $f'(0)f'''(0) > 0$, the Hopf bifurcation is subcritical. If $f'(0)f'''(0) < 0$, the Hopf bifurcation is supercritical.*

(2) *There are no cubic terms in the Taylor expansion of the nonlinearity: If $f'''(0) = 0$ and $f''(0) \neq 0$, then the Hopf bifurcation is subcritical if $C^n(\tau, r) > 0$ and supercritical if $C^n(\tau, r) < 0$.*

In this section, we provide in Proposition 1 a criterion that determines the type of Hopf bifurcation in general but requires the numerical evaluation of the function $C^n(\tau, r)$. The Hopf bifurcation type can be determined without the evaluation of $C^n(\tau, r)$ if certain assumptions about the parameters of model (3) are satisfied (see corollary 2 and also [Illing]).

To illustrate the theoretical findings, we consider the specific example of the opto-electronic time-delay feedback systems with band-limited feedback described in Sec. 2, where a supercritical Hopf bifurcation was found. The nonlinearity f of the experiment, given by Eq. (4), is such that the experiment does not fall into one of the simple cases of Corollary 2, necessitating a numerical evaluation of $C^n(\tau, r)$, which reveals that $f'(0)f''(0) + f''(0)^2 C^n(\tau, r) < 0$. Thus, the bifurcation is predicted to be supercritical, in agreement with the experimental result.

4 Summary and Conclusion

This paper focuses on the class of time-delay systems that are characterized by a passive nonlinearity and a band-limited feedback. We describe an opto-electronic device with band-limited feedback that operates in the megahertz frequency range and that allows adjustment of the characteristic time scale of the oscillations by changing the band-pass characteristics of the feedback loop. We show that the periodic oscillations in the device arise through Hopf bifurcations and provide evidence that the observed device dynamics for large feedback-gains are due to deterministic chaos. We study theoretically the general model for time-delay systems with band-limited feedback and show that Hopf-bifurcations of the steady state are a generic feature of such systems. Furthermore, we provide a criterion that determines whether the Hopf-bifurcation is supercritical or subcritical.

We find that the inclusion of a high-pass filter in the feedback loop significantly changes the qualitative dynamics of optical feedback systems with passive nonlinearity in comparison to only low-pass filtering as in the Ikeda system [Ikeda, 1982]. Bandpass feedback allows not only "fundamental" frequencies $f \sim (2\tau)^{-1}$ but oscillations with $f \sim \tau^{-1}$ become possible. The route to chaos is apparently changed when the feedback of DC-signals is blocked. That is, we do not observe a period doubling route to chaos but a more complicated transition, the details of which are not yet fully understood.

References

Abarbanel, H. D. I., Kennel, M., Illing, L., Tang, S., Chen, H. F. and Liu. J. M. (2001) Synchronization and Communication Using Semiconductor Lasers With Optoelectronic Feedback, *IEEE J. Quantum Electron.*, **37**, pp. 1301-1311.

Blakely, J. N., Illing, L. and Gauthier, D. J. (2004a) High-Speed Chaos in an Optical Feedback System With Flexible Timescales, *IEEE J. Quantum Electron.*, **40**, pp. 299-305.

Blakely, J. N., Illing, L. and Gauthier, D. J. (2004b) Controlling Fast Chaos, *Phys. Rev. Lett.*, **92**, pp. 193901.

Derstine, M. W., Gibbs, H. M., Hopf, F. A. and Kaplan, D. L. (1983) Alternate paths to chaos in optical bistability, *Phys. Rev. A*, **27**, pp. 3200-3208.

Dronov, V., Hendrey, M. R., Antonsen, Jr., T.M. and Ott, E. (2004) Communication with a chaotic traveling wave tube microwave generator, *Chaos*, **14**, pp. 30-37.

Erneux, T., Larger, L., Lee, M. W. and Goedgebuer, J. P. (2004) Ikeda Hopf bifurcation revisited, *Physica D*, **194**, pp. 49-64.

Faria T. and Magalhães, L. T. (1995) Normal form for retarded functional differential equations with parameters and applications to Hopf singularity, *J. Differ. Equations*, **122**, pp. 181-200.

Fischer, I., Liu, Y. and Davis, P. (2002) Synchronization of chaotic semiconductor laser dynamics on subnanosecond time scales and its potential for chaos communication, *Phys. Rev. A*, **62**, pp. 011801

Garcia-Ojalvo, J. and Roy, R. (1996) Noise amplification in a stochastic Ikeda model, *Phys. Lett. A*, **224**, pp. 51-56.

Giannakopoulos, F. and Zapp, A. (1999) Local and Global Hopf Bifurcation in a Scalar Delay Differential Equation, *J. Math. Anal. Appl.*, **237**, pp. 425-450.

Guckenheimer, J., and Holmes, P. (1983) *Nonlinear Oscillations, Dynamical Systems, and Bifurcations of Vector Fields*, Springer-Verlag, New York.

J. P. Goedgebuer, J. P., Larger, L., Porte, H., Delorme, F. (1998) Chaos in wavelength with a feedback tunable laser diode, *Phys. Rev. E*, **57**, pp. 2795-2798.

Goedgebuer, J. P., Levy, P., Larger, L., Chen, C. C. and Rhodes, W. T. (2002) Optical Communication With Synchronized Hyperchaos Generated Electrooptically, *IEEE J. Quantum Electron.*, **38**, pp. 1178-83.

Genin, É., Larger, L., Goedgebuer, J. P., Lee, M. W., Ferriére, R. and Bavard, X. (2004) Chaotic Oscillations of the Optical Phase for Multigigahertz-Bandwidth Secure Communications, *IEEE J. Quantum Electron.*, **40**, pp. 294-298.

Hale, J. K. and Verduyn-Lunel, S. M. (1993) Introduction to Functional Differential Equations, Springer-Verlag, New York.

Hale, J. K. and Huang, W. (1996) Periodic solutions of singularly perturbed delay equations, *Z. angew. Math. Phys.*, **47**, pp. 57-88.

Hale, J. K., Magalhães, L. T., and Oliva, W. L. (2002) *Dynamics in Infinite Dimensions, 2nd ed.*, Springer-Verlag, New York.

Ikeda, K. (1979) Multiple-valued stationary state and its instability of the transmitted light by a ring cavity, *Opt. Commun.*, **30**, pp. 257-261.

Ikeda, K. and Kondo, K. (1982) Successive higher-harmonic bifurcations in systems with delayed feedback *Phys. Rev. Lett.*, **49**, pp. 1467-70.

Ikeda, K. and Matsumoto, K. (1987) High-dimensional chaotic behavior in systems with time-delayed feedback, *Physica D*, **29**, pp. 223-235.

Illing, L. and Gauthier, J. D., submitted for publication.

Kobayashi, S., Yamamoto, Y., Ito, M. and Kimura, T. (1982) Direct frequency modulation in AlGaAs semiconductor lasers, *IEEE J. Quantum Electron.*, **18**, pp. 582-95.

K. Kusumoto, K. and Ohtsubo, J. [2002] 1.5 GHz message transmission based on synchronization of chaos in semiconductor lasers, *Opt. Lett.*, **27**, pp. 989-91.

Liu, Y. and Ohtsubo, J. (1991) Observation of higher harmonic bifurcations in a chaotic system using a laser diode active interferometer, *Opt. Commun.*, **85**, pp. 457-461.

Lukin, K. A., Cerdeira, H. A., Colavita, A. A. (1997) Chaotic instability of currents in a reverse biased multilayered structure, *Appl. Phys. Lett.*, **71**, pp. 2484-2486.

Mykolaitis, G., Tamaševičius, A. , Čenys, A., Bumeliene, S. ,Anagnostopoulos, A. N. and Kalkan, N. (2003) Very high and ultrahigh frequency hyperchaotic oscillator with delay line, *Chaos Solitons Fractals*,**17**, pp. 343-347.

Myneni, K., Barr, T. A., Reed, B. R. ,Pethel,S. D. ,Corron, N. J. (2001) High-precision ranging using chaotic laser pulse train, *Appl. Phys. Lett.*, **78**, pp. 1496-1498.

Nardone, P. Mandel, P. and Kapral, R. (1986) Analysis of a delay-differential equation in optical bistability, *Phys. Rev. A*, **33**, pp. 2465-2471.

Nizette, M. (2004) Front Dynamics in a delayed-feedback system with external forcing, *Physica D*, **183**, pp. 220-244.

Pyragas, K. (1992) Continuous control of chaos by self-controlling feedback, *Phys. Lett. A*, **170**, pp. 412-428.

Socolar, J. E. S., Sukow, D. W. and Gauthier, D. J. (1994) Stabilizing unstable periodic orbits in fast dynamical systems, *Phys. Rev. E*, **50**, 3245-3248.

S. H. Strogatz (1994) *Nonlinear Dynamics and Chaos*, Perseus Books Publishing, pp. 264.

Tsai, C. Y., Chen, C. H., Sung, T. L., Tsai, C. Y. and Rorison, J. M. (1999) Theoretical modeling of carrier and lattice heating effects for frequency chirping in semiconductor lasers, *Appl. Phys. Lett.*, **74**, pp. 917-919.

VanWiggeren, G. D. and Roy, R. (1998) Communication with chaotic lasers, *Science*, **279**, pp. 1198-1200.